Morphological Development of Oriented Isotactic Polypropylene in the Presence of a Nucleating Agent

Peng-wei Zhu,* Jason Tung, Andrew Phillips, and Graham Edward

Department of Materials Engineering, CRC for Polymers, Monash University, Vic 3800, Australia

Received November 8, 2005; Revised Manuscript Received January 16, 2006

ABSTRACT: The morphological development of sheared isotactic polypropylene (iPP) containing different amounts of sodium benzoate (SB) has been investigated using wide- and small-angle X-ray scattering techniques. The microbeam of synchrotron radiation allows us to gain, precisely and efficiently, the local morphology at a given position with a good spatial resolution. The morphological distributions such as crystallinity, fractions of α-form and *β*-form crystals, crystal size, and orientation functions can therefore be well constructed through the shear field or temperature gradient. The distribution of crystallinity is changed from a U-shape without SB to an almost flat with SB, in company with a minimum fraction of α-form crystal and a maximum fraction of *β*-form crystal. The epitaxial growth of branched lamellae in the presence of SB is confirmed from the orientation functions of two axes using wide-angle diffraction. The effect of SB on the molecular orientation is understood from the orientation function of *c*-axis and the azimuthal patterns of small-angle scattering. It is found that both the molecular orientation and the lamellar orientation of the α-form crystal are increased with increasing SB. The thickness of crystalline lamellae with respect to flow direction is found to increase with increasing SB in the whole range from shear zone to core center. A slight declination of crystalline lamellae has been observed in the presence of SB.

Introduction

In an injection molding of semicrystalline polymers, molten polymers are exposed to varying levels of a shear flow field and a temperature gradient prior to the crystallization. The resulting morphology is thus quite different from what is observed under the quiescent condition. Typically, multiple layers or a skin−core structure[1−14] of semicrystalline polymers can form during the injection molding. The very thin skin region is essentially an amorphous phase due to a rapid cooling. The broad core region contains a spherulitic structure because the lower cooling rate and lower shear-strain history allow a complete relaxation of chain molecules. A shear zone or surface region separates the skin and core regions and is a most important part determining shear-induced properties. In particular, a "shish-kebab" structure, a special kind of polymer crystalline assembly, can form in the shear zone under the certain molding conditions.[15−18]

A number of models were proposed to describe the special morphology of isotactic polypropylene (iPP) during or after the imposition of shear flow. From studies of the injection-molded iPP, Clark et al. suggested that the sheared iPP lamellae have a mixed *c*-axis and *a**-axis orientation or bimodal in the shear zone.[7] The *c*-axis here is referred to the lamellae having their folding chains or *c*-axis preferentially aligned along the flow direction whereas the *a**-axis referred to the lamellae having their folding chains preferentially perpendicular to the flow direction. The *c*-axis-oriented components are expected to form first, and then the *a**-axis-oriented components epitaxially grow on the substrate of *c*-axis-oriented components. This bimodal morphology is conceptually similar to the "parent−daughter" model, and the full details of epitaxial mechanism at the molecular level have been given in the literature.[19] In the line with this work, it has been suggested that, in addition to the main skeleton of the shish-kebab structure, some of the kebabs or *c*-axis-oriented components would be connected each other.[10] The structure of injection-molded iPP at the level of lamellae can be schematically shown in Figure 1.

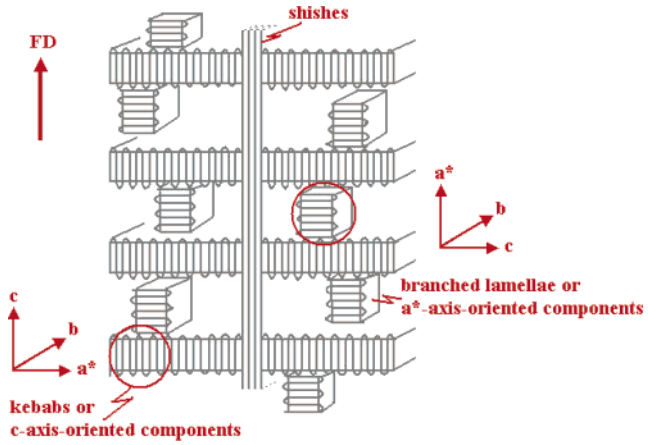

Figure 1. Schematic diagram of branched shish-kebab structure of Fujiyama et al.[10]

Although the morphology of injection-molded semicrystalline polymers has been widely studied, much experimental work has been mainly devoted to the effects of processing conditions of shear flow, such as temperature, deformation strain, and deformation rate, on the resulting morphology. Among industrial applications, on the other hand, it is not uncommon that suitable nucleating agents are added into polymers during the operation of injection molding. Nucleating agents are used not only because they can significantly increase the crystallization rate of molten polymers and therefore the rate of production of artifacts, but also because they would dramatically and selectively alter the solid-state morphology of sheared polymers and, therewith, improve physical, mechanical, and optical properties.[20] A variety of nucleating agents have been designed to tailor the structures.[20,21] The addition of nucleating agent molecules into sheared polymer melts will certainly complicate the crystallization process and the morphology that subsequently forms.[21−26]

In the present work, the influence of sodium benzoate (SB) on the morphologies and morphological distributions of

10.1021/ma052375g CCC: $33.50
Published on Web 02/08/2006

injection-molded iPP is further studied by means of synchrotron wide-angle X-ray diffraction (WAXD) and small-angle X-ray scattering (SAXS). Such studies cannot be directly carried out using conventional X-ray because its beam size is so big that both the shear region and the core region are illuminated. A microbeam of synchrotron radiation allows the morphologies from the shear region to the core region to be positioned, precisely and efficiently, and the morphological development along the shear field and temperature gradient can be well constructed. Sodium benzoate is a nucleating agent with some functions such as antimicrobial, flavoring, and acid acceptor. The flow-induced crystallization of semicrystalline polymers can be studied in a broad range of shearing rates using thin samples in a laboratory scale. In the present work, the molten iPP is sheared in a truly industrial process, and iPP is expected to be under a weak level of shear in a broad range.

Experimental Section

A commercial isotactic polypropylene and SB were kindly provided by Basell, Australia. The molecular weight of iPP was determined by using gel permeation chromatography in 1,2,4-trichlorobenzene with antioxidant at 160 °C. The average weight molecular weight M_w and the average number molecular weight M_n are 260 000 and 41 200, respectively. SB was mixed with iPP in a small single-screw extruder at a SB concentration of 4.0 wt % to produce a masterbatch. The masterbatch was pelletized and further extruded to improve the dispersion and distribution of the SB. This was then mixed with further iPP in the extruder to produce different concentrations of SB. Rectangular plates of iPP were injection molded with molding conditions as follows: melt temperature 220 °C, mold temperature 60 °C, holding pressure 250 bar, holding time 3.8 s, cooling time 40 s, and flow front velocity 2 cm/s through the cavity.

Differential scanning calorimetry (DSC) was performed using a Perkin-Elmer Pyris1 instrument with a heating rate of 10 °C/min. The temperature scale was routinely calibrated using indium and zinc standards. The samples were sealed in aluminum pans, and the typical sample weight was about 8−10 mg.

The synchrotron experiments were performed at room temperature at the Australian National Beamline Facility (ANBF) in Tsukuba of Japan. The ANBF is installed on a bending magnet port and delivers monochromatic synchrotron X-rays in the energy range 4.5−20 keV to the experimental station in a hutch. The instrument has a multiconfiguration vacuum diffractometer that uses image plates as its detector system. The square-shaped beam had dimensions of 200 × 200 μm^2. The wavelengths of 2.0 and 1.0 Å were respectively employed to record 2D SAXS and WAXD image patterns.

The injection-molded iPP specimens were cut at a central position away from the gate with a length of 10 mm, a thickness of 1.0 mm, and a width of 2.6 mm. These specimens were named iPP-0.0, iPP-0.1, iPP-0.4, and iPP-1.2, corresponding respectively to the SB concentrations of 0, 0.1, 0.4, and 1.2 wt %. The thin iPP specimens with surfaces parallel to the flow direction were also cut using a microtome, and the crystalline texture was observed using a polarizing microscope. For the present work, however, the quantitative information on the morphological development cannot be obtained from the polarizing microscope.

The iPP specimens were mounted at the center of ANBF vacuum diffractometer with the specimens 570 mm from the image plate. Measurements were performed with the primary beam being perpendicular to the flow direction and the scattering being measured along a direction normal to the layered planes in the molding. The beam passed through the specimen, and the illuminated zone was changed with a vertical shift of the sample holder along the direction of plate thickness (or specimen width). Only one half-width of each specimen was illuminated on the assumption that the morphology at the same distance from the surfaces of a plate is the same or the morphological distribution is symmetrical. Physical parameters calculated later were plotted as a function of the depth through the plate thickness. For all specimens, the first measurement was always taken with the beam center 100 μm from the surface. The intensity at 100 μm is therefore low simply because the illuminated area is smaller. This step should not be taken as a measurement of the skin as the beam cannot access the pure skin. The integrated intensity of image patterns was obtained using PPDA software. The scattered intensity of SAXS was presented as a function of scattering vector q where $q = 4\pi \sin(\theta)/\lambda$. Scattering without the specimen was recorded as a background to enable correction of measured SAXS patterns.

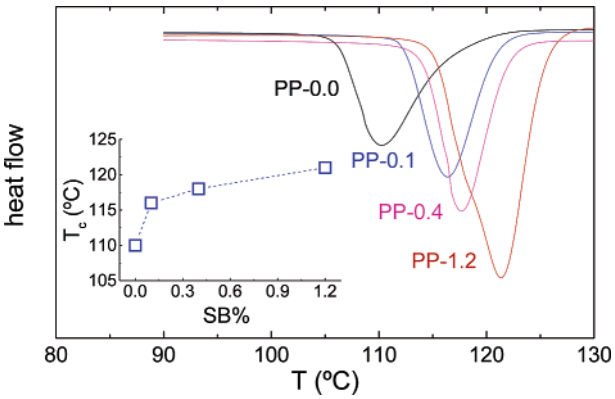

Figure 2. DSC scans in a cooling for samples containing different concentrations of SB. The inset is a plot of crystallization temperature as a function of concentration of SB.

Results

Differential Scanning Calorimetry and Crystallization Temperature. Figure 2 shows DSC cooling thermograms obtained after holding at 180 °C for 3 min. The crystallization temperature, T_c, obtained from the minimum of exothermic crystallization peak is about 110 °C for iPP-0.0. The addition of only 0.1% SB into iPP leads to a marked shift of crystallization peak toward a higher temperature, T_c = 116 °C. T_c increases with a further increase in SB, and no saturation in T_c is observed in the range of SB concentration studied. DSC heating thermograms show that the melting temperature T_m obtained is the almost same within the error of experiments, irrespective of SB concentration. The DSC results indicate that the supercooling $\Delta T = (T_m^0 - T_c)$ of shear-induced crystallization decreases with increasing SB, where T_m^0 is an equilibrium melting temperature. The resulting morphological development under the different supercooling is expected to be different.

WAXD Image Patterns and Distribution of Crystallinity. Figure 3 typically shows WAXD image patterns obtained from different depths of iPP-0.0 and iPP-1.2 plates. 1D WAXD profiles were obtained from circularly integrated intensities of 2D WAXD image patterns in order that the effect of molecular orientation can be included. Figure 4 shows 1D WAXD profiles from the samples iPP-0.0 and iPP-1.2. The main reflection peaks correspond to the α- and β-form crystals. A series of Bragg peaks observed from iPP-1.2 are well consistent with corresponding ones from iPP-0.0, suggesting that the polymer's unit cell is not significantly modified by the presence of SB molecules.

A peak-fit procedure was used to deconvolute the peaks of 1D WAXD profiles. A typical profile is shown in Figure 5. The Gaussian function was used to describe the amorphous and crystal peaks, except for the α(110) peak. The application of the Lorentz function to the α(110) peak is found to give a better

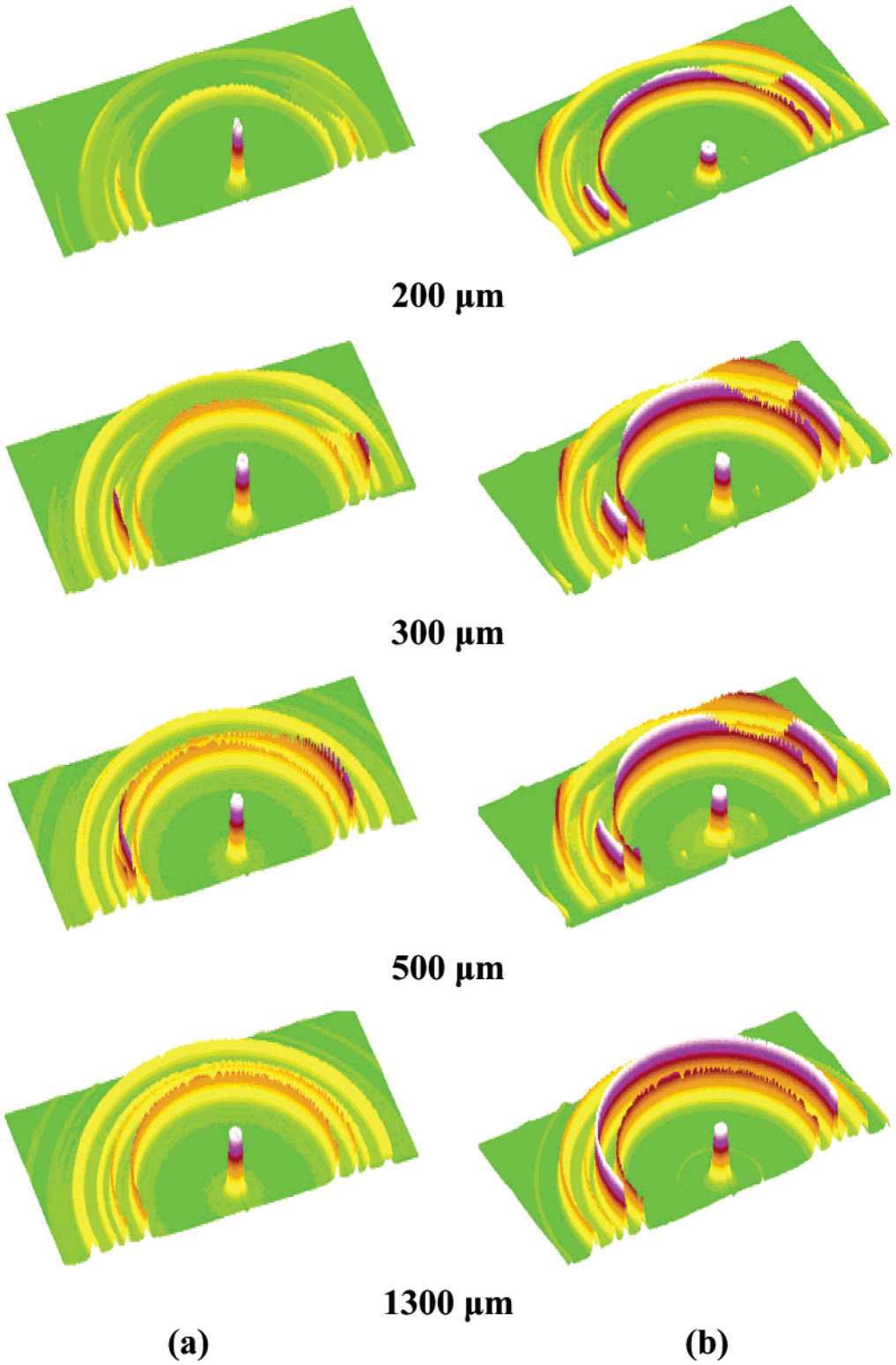

Figure 3. WAXD image patterns at different distances from the surface of plates for (a) iPP-0.0 and (b) iPP-1.2.

fit of whole curve. The overall crystallinity X_c is calculated by

$$X_c = \frac{\sum A_{cryst}}{\sum A_{cryst} + \sum A_{amorp}} \quad (1)$$

where A_{cryst} and A_{amorp} are the fitted areas of crystal and amorphous, respectively. The relative amount of the β-form crystal, K_β, in the crystalline portion of the sheared iPP can be evaluated by the Turner-Jones criterion[27] defined as follows:

$$K_\beta = \frac{A_\beta(300)}{A_\beta(300) + A_\alpha(110) + A_\alpha(040) + A_\alpha(130)} \quad (2)$$

where $A_{\Omega(hkl)}$ represents the area of the *(hkl)* peak belonging to the phase Ω (α- or β-form crystal). The crystallinity of the β-form crystal X_β and the crystallinity of the α-form

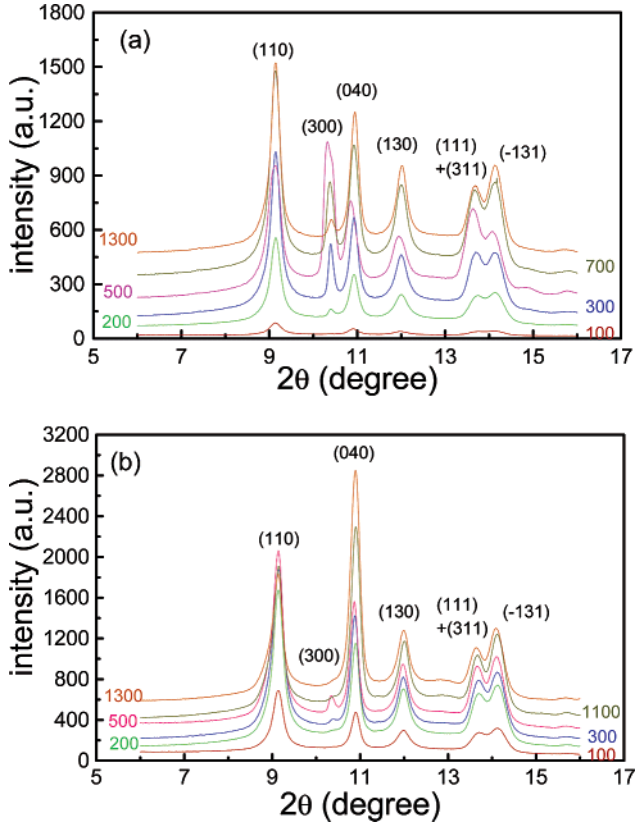

Figure 4. Plots of WAXD intensity as a function of 2θ for (a) iPP-0.0 and (b) iPP-1.2. The intensity is calculated from a circulated integration of Figure 3. The number of each trace indicates the distance from the surface of injection-molded plates.

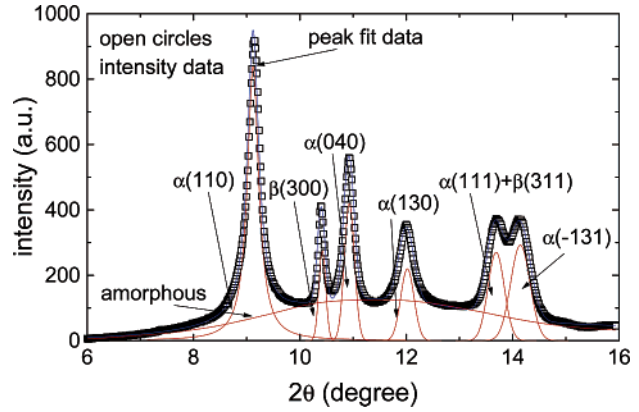

Figure 5. Deconvolution of an example WAXD intensity profile for the calculation of total crystallinity and contributions of α-form crystal and β-form crystal.

crystal X_α are respectively given by

$$X_\beta = K_\beta X_c \tag{3}$$

$$X_\alpha = X_c - X_\beta \tag{4}$$

Figure 6 shows the distributions of overall crystallinity X_c through the depth of iPP plates. There are two types of X_c distribution, depending on the SB concentration. For iPP-0.0 and iPP-0.1, the variation of X_c with the depth can be described as a U-shape. Higher levels of shear result in, as expected, higher degrees of overall crystallinity. In the cases of iPP-0.4 and iPP-1.2, on the other hand, a higher level of shear flow does not necessarily give a higher value of X_c, although a subtle change in X_c is imprinted as the influence of shear flow. In general,

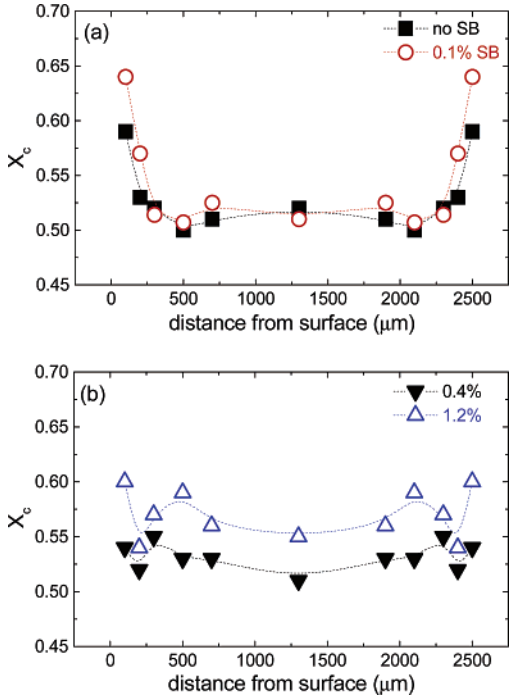

Figure 6. Distributions of volume crystallinity for the samples containing different concentrations of SB.

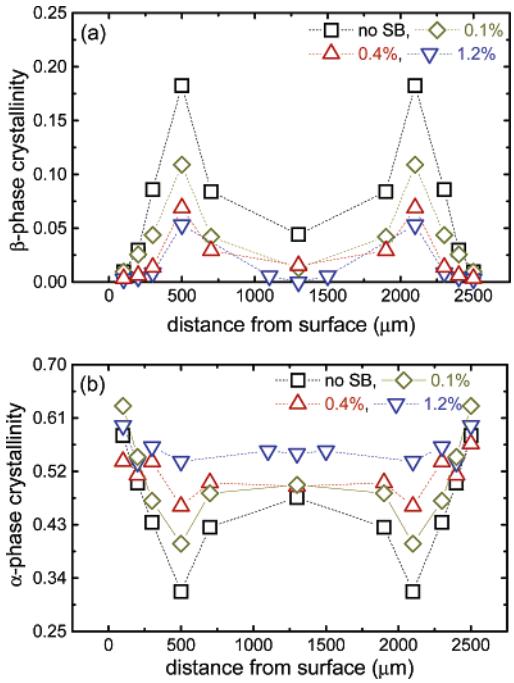

Figure 7. Distributions of volume crystallinity of α-form crystal and volume crystallinity of β-form crystal for the samples containing different concentrations of SB.

the distribution of X_c in iPP-0.4 and iPP-1.2 tends to be a flat. It is worth noting, however, that overall crystallinity of iPP-1.2 increases over a broad range.

Figure 7 shows the crystallinity distributions of α- and β-form crystals through the depth of iPP plates. A number of features about the changes in the crystals are evident. (i) With an increase in SB, the crystallinity of α-form crystal increases, while the crystallinity of β-form crystal decreases. This is due to the fact that the SB is capable of selectively nucleating the α-form crystal. (ii) The β-form crystal is sensitive to the level of shear. As can be seen, X_β always varies with the depth or equivalently

the level of shear, irrespective of the SB concentration. In contrast, the influence of shear flow on X_α tends to attenuate with increasing SB. The increase in X_α with SB is attributed to the flat distribution of X_c. (iii) The minimum X_α is observed at the same depth as the maximum X_β. Particularly, they appear at 500 μm rather than the core center where the level of shear flow is negligible.

Hermans Orientation Function and Distribution of Molecular Orientation. A quantitative measure of molecular orientation in crystalline iPP can be calculated from WAXD using the Hermans orientation function defined as follows:

$$f_H = \frac{3\langle\cos^2\varphi\rangle - 1}{2} \tag{5}$$

where φ is an angle between the unit within a crystal of interest (e.g., *c*-axis) and a reference axis (flow direction in the present work), and $\langle\cos^2\varphi\rangle$ is defined as

$$\langle\cos^2\varphi\rangle = \frac{\int_0^{\pi/2} I(\varphi)\cos^2\varphi\sin\varphi\,d\varphi}{\int_0^{\pi/2} I(\varphi)\sin\varphi\,d\varphi} \tag{6}$$

In the present work, we are interested in the *c*-axis (or the fold chain) parallel to the flow direction. Assuming the rotational symmetry around the flow direction and defining the angles ω, μ, and σ in *a**-, *b*-, and *c*-axis with the flow direction, the orientation functions are given by

$$f_{a^*} = \frac{3\langle\cos^2\omega\rangle - 1}{2} \tag{7}$$

$$f_b = \frac{3\langle\cos^2\mu\rangle - 1}{2} \tag{8}$$

$$f_c = \frac{3\langle\cos^2\sigma\rangle - 1}{2} \tag{9}$$

with

$$f_{a^*} + f_b + f_c = 0 \tag{10}$$

The *b*-axis orientation f_b of α-form crystal can be directly calculated from the measured WAXD (040) reflection by

$$\langle\cos^2\mu\rangle = \langle\cos^2\varphi_{(040)}\rangle \tag{11}$$

Because there is no a pure reflection from *c*-axis of iPP, the *c*-axis orientation f_c of α-form crystal is calculated using Wilchinsky's method[28] from unit cell geometry and the diffraction intensities from strong (110) and (040) reflections:

$$\langle\cos^2\sigma\rangle = 1 - 1.099\langle\cos^2\varphi_{(110)}\rangle - 0.901\langle\cos^2\varphi_{(040)}\rangle \tag{12}$$

The *a**-axis orientation f_{a^*} can be obtained from eq 10. Physically, the Hermans orientation function f_H has a value of unity when all the crystals are oriented parallel to the reference direction that is coincident to the flow direction in the present system. f_H has a value of −0.5 when it is oriented perpendicularly to the reference direction and a value of 0 for a random orientation.

Figure 8 shows the distributions of Hermans orientation functions of α-form crystal through the depth of the plates. The values of *c*-axis orientation function f_c of iPP-0.0 are positive.

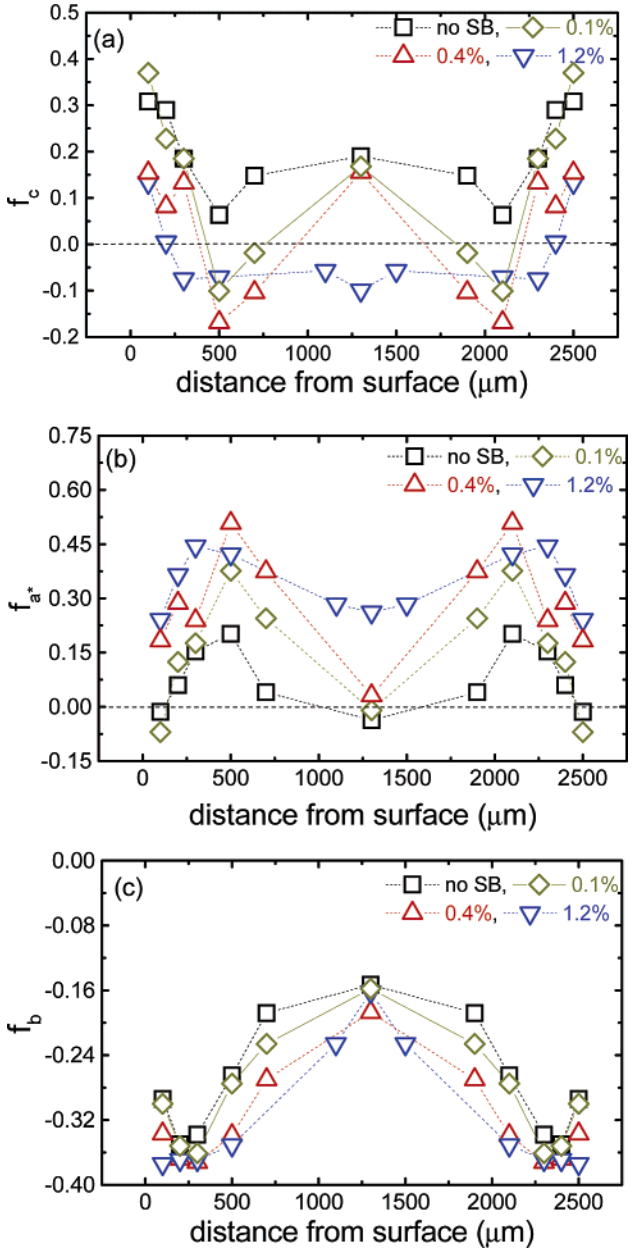

Figure 8. Distributions of orientation functions for the samples containing different concentrations of SB.

However, as the concentration of SB increases, the value of f_c decreases and even changes the sign to negative. Especially, over a broad range, the f_c values of iPP-1.2 are negative but close to zero, a "random orientation" as its definition. In opposition to f_c, however, the value of *a**-axis orientation function f_{a^*} always increases with increasing SB. Note that the f_{a^*} value of iPP-0.0 is close to zero not only in the core center where the shear is negligible, if anything, but also at 100 μm where the molten polymer should be imposed by a high level of shear flow. Furthermore, the maximum f_{a^*} and the minimum f_c are observed at 500 μm where, as seen above, the minimum X_α and the maximum X_β appear. These results reveal that sheared iPP melt can be modified over the whole range, and the flow behavior is more complicated than normally thought. It should be particularly pointed out that the orientation function of *c*-axis alone cannot be used to measure the molecular orientation with respect to the flow direction for the branched shish-kebab (or the parent−daughter) structure. As can be seen from Figure 1, the values of f_c and f_{a^*} include the orientation

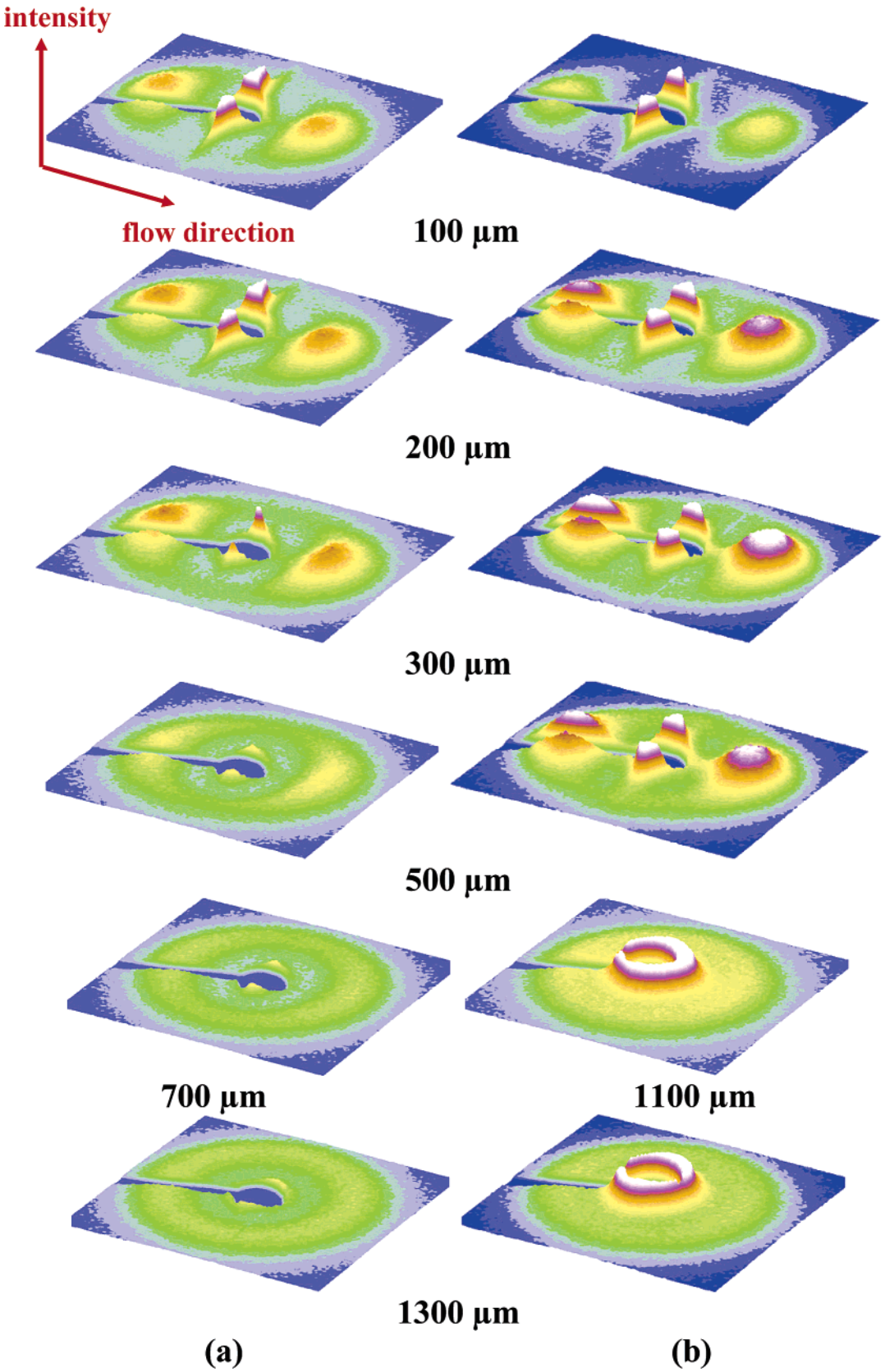

Figure 9. SAXS image patterns at different distances from the surface of plates for (a) iPP-0.0 and (b) iPP-1.2.

contributions from both the *c*-axis-oriented components and the *a**-axis-oriented components. As will be seen later from SAXS, even if the value of f_c is zero, the chain orientation should not be at random.

All the values of f_b have a negative sign, as shown in Figure 8c. This is understandable because the *b*-axis inclines perpendicularly to the flow direction. According to Figure 1, the growth axis is the *a**-axis and the lamellae stack up through the *b*-axis direction. It is found that from the core center to the shear region the value of f_b can be changed from ~−0.16 to ~−0.35. Since the *b*-axis of *c*-axis-oriented components is parallel to that of *a**-axis-oriented components, as seen in Figure 1, Figure 8c

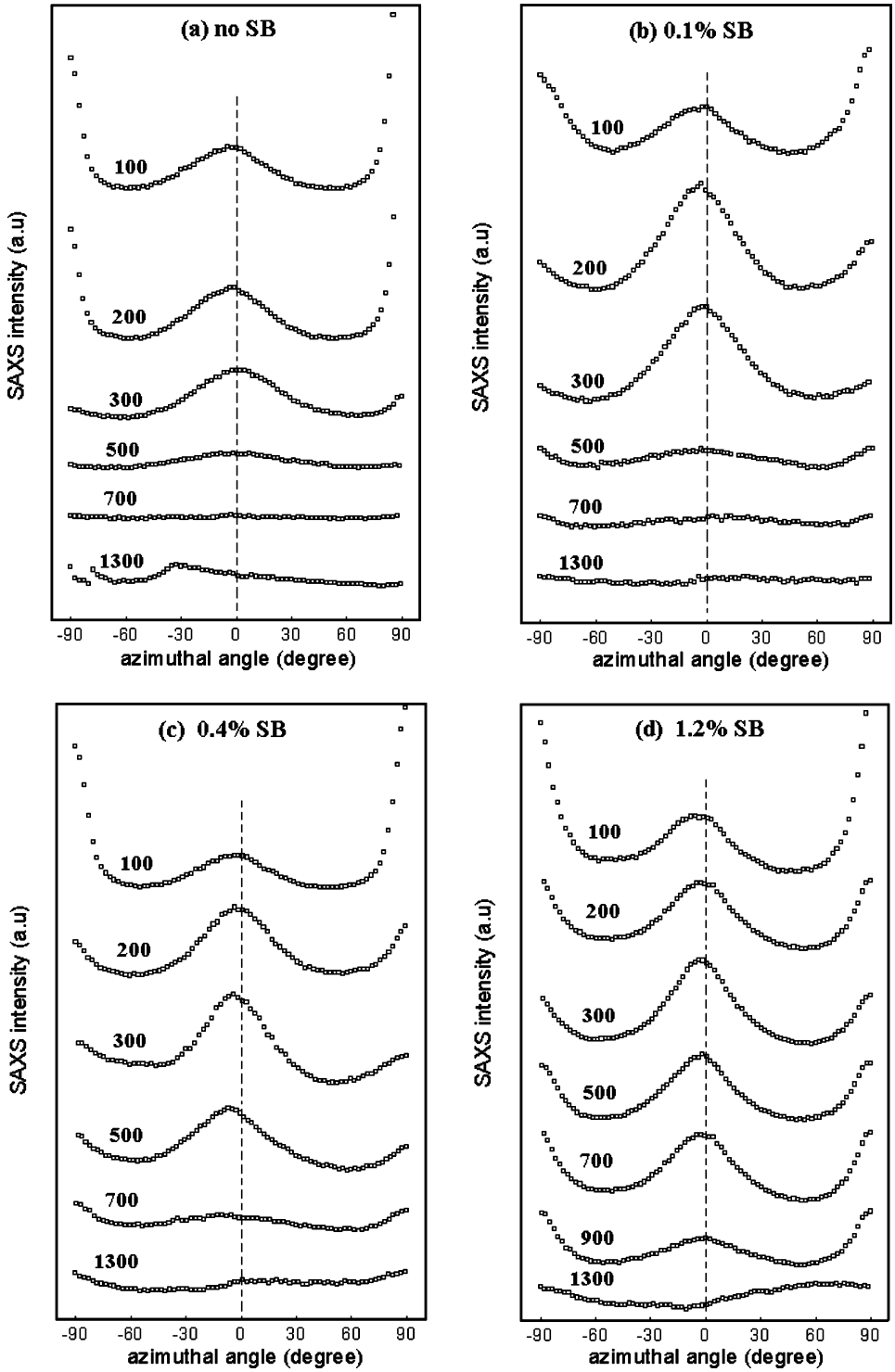

Figure 10. Azimuthal patterns of SAXS for the samples containing different concentrations of SB. The number of each trace indicates the distance from the surface of injection-molded plates.

reveals that the shear can effectively induce the *b*-axis preferentially perpendicular to the flow direction, and particularly, the higher concentration of SB leads to higher levels of *b*-axis orientation.

SAXS Image Patterns and Distribution of Lamellar Orientation. Figure 9 shows the SAXS image patterns through the depths of iPP-0.0 and iPP-1.2 plates. Four scattering spots along and normal to the flow direction are observed. The image patterns are partially obscured by the beam stop. The lamellar orientation with respect to the flow direction is evidenced by the variation of the meridian spots. As the depth is increased toward the core center, the spot intense and height continue reducing, indicating the influence of shear flow on the lamellar orientation. On the other hand, the lamellar orientation at a given depth is remarkably enhanced by the addition of SB. Even in the core center, the ring intensity of iPP-1.2 is much stronger than that of iPP-0.0.

Figure 10 shows the distributions of azimuthal SAXS patterns through the depth for the samples containing different concentrations of SB. Each azimuthal pattern represents SAXS data collected over a shear decrement from the shear region to the core region. The absence of intensity variation means that the

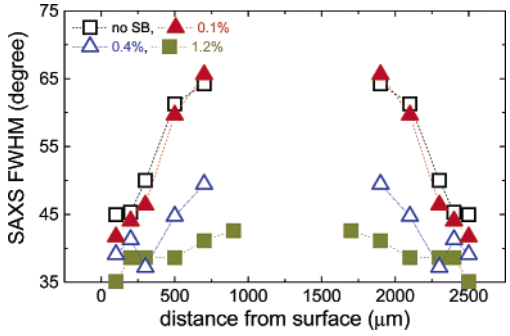

Figure 11. Distributions of the full width at half-maximum (fwhm) for the samples containing different concentrations of SB.

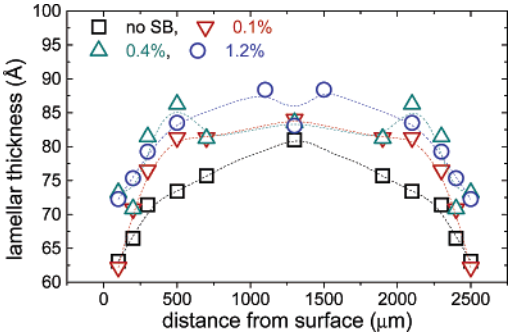

Figure 12. Distributions of the thickness of crystalline lamellae for the samples containing different concentrations of SB.

crystalline lamellae possess no preferred orientation. It can be seen from Figure 10 that at 200 μm, for an example, the lamellar orientation of iPP-1.2 is very significant even though the f_c of iPP-1.2 is equal to zero at the same position (see Figure 8a). To describe quantitatively the lamellar orientation and corresponding distribution, the full width at half-maximum (fwhm) of the main peak was calculated. The results obtained are presented in Figure 11. The increase in fwhm with the depth indicates the decrease in the level of lamellar orientation due to the attenuation of shear flow. At a given position, the results show the SB-enhanced orientation of crystalline lamellae.

It is worth noting from Figure 11 that the maximum of the main peak of iPP-0.0 deviates, though subtly, from $\varphi = 0°$ at 100 μm where the level of shear is expected to be maximum. For the other samples, this phenomenon appears not only at 100 μm but also other positions. This observation reveals that the morphological development would be involved in an inclination of oriented lamellae (or kebabs) about the shish walls, though weak, under higher levels of shear flow or probably the local flow perturbation.

Distribution of Thickness of Crystalline Lamellae. If a crystallite size is small, its size can be calculated from diffraction peaks of WAXD using the Scherrer equation[29]

$$L_{hkl} = \frac{K\lambda}{\beta_{hkl}\cos\theta_{hkl}} \tag{13}$$

where L_{hkl} is the crystallite size in the direction perpendicular to the diffraction plane (hkl), K is crystallite shape factor (0.89), and $\beta_{hkl} = (B_{hkl}^2 - b_0^2)^{1/2}$, with B_{hkl} being a peak width at half-maximum intensity and b_0 the instrumental resolution. The assumption in the Scherrer equation is that all the line broadening of reflections results from the finite crystallite size. L_{001} has to be estimated from the reflections (111), (041), and (−131) of α-form crystals due to the absence of a pure reflection from (00l). The thickness of crystalline lamellae parallel to the flow direction, L_{001}, calculated from the reflection (−131) is thus given as follows:

$$L_{001} = L_{\bar{1}31}\cos\omega = \frac{K\lambda}{\beta_{\bar{1}31}\cos\theta_{\bar{1}31}}\cos\omega \tag{14}$$

where ω is an angle between the lattice planes (001) and (−131). Using the crystal unit cell of the α-form crystal ($a = 6.66$ Å, $b = 20.78$ Å, $c = 6.495$ Å, $\beta = 99.62°$, and $\alpha = \gamma = 90°$),[30] the value of ω was calculated to be 57.89°. For the present work, the crystallite size L_{001} is equivalent to the thickness of crystalline lamellae with their fold chains parallel to the flow direction. It is worth pointing out that the thickness calculated from WAXS is the one of extended chains within fold chain lamellae, and it should be smaller than that determined by SAXS.

Figure 12 shows the distribution of thickness of crystalline lamellae through the depth. The thickness of crystalline lamellae is smaller in the shear region than that in the core region, regardless of SB concentration. As the concentration of SB is increased, the thickness of crystalline lamellae tends to increase. In the core center, the lamellar thickening in crystalline phase is almost independent of SB, although the molecular and the lamellar orientations are not at the same level.

Discussion

The morphological development during an injection molding is governed by the temperature and shear flow. In addition to the control parameters related to the processing conditions of injection molding, the important morphology-related parameters to consider include the temperature gradient (or the cooling rate) of molding, the crystallization temperature of samples or supercooling, and the shear stress at the solid/melt interfaces cross the temperature gradient. The thermal level Y can be defined as follows:[5]

$$Y = \frac{T_b - T_c}{T_b - T_i} \tag{15}$$

where T_b and T_i are an average melt temperature (or bulk temperature) and a local melt temperature, respectively. A low thermal level in general corresponds to a high level of shear through the direction of thickness. The morphological development is determined by the consequence of an intricate balance between shear flow and thermal level.

In the shear region, the chain segments tend to be more easily locked or frozen through a way in which they are first incorporated due to the higher cooling rate or the lower thermal level, which, like a quasi-quenching, causes the lower degree of crystallinity. On the other hand, the level of shear flow is sufficient to induce the higher growth rate of crystallization and the higher nucleation density[31] that should favor the higher degree of crystallinity. The U-shape distribution of overall crystallinity X_c in iPP-0.0 suggests that the shear is a dominant factor over X_c in the shear region. The crystallization in the core region is expected to undergo mainly in a quiescent condition because the shear flow imposed on melt is weak. The cooling rate is thus a governing factor. The thermal environment was certainly modified to some extent by the addition of SB due to the increase in T_c. In respect of X_c only, however, the amount of SB in iPP-0.1 is not sufficient to cause the change in the distribution.

The distribution of X_c changed from U-shape to flat is largely due to the increase in X_c of the core region. Since the degree of

crystallinity increases with increasing thermal level,[5] the decrease in $(T_b - T_c)$ due to the increase in T_c in the core region should accompany the more decrease in $(T_b - T_i)$. The higher diffusion rate of chains toward crystallizing germs and an ordering processing would also be taken into account. Unlike the core region where the thermal level is dominant, the value of X_c in the shear region is a consequence of the balance between the lower thermal level and the higher shearing.

The increase in X_c is consistent with the thickening of crystalline lamellae. In the presence of nucleating agent, the effect of ΔT on the thickness of a crystalline lamella, L_c, can be given, in a simplest way, as follows:[21,32]

$$L_c = 2\sigma_e \frac{\upsilon_c T_m^0}{\Delta H_f (T_m^0 - T_c)} \tag{16}$$

with

$$\sigma_e = \sigma_{e0}\left(1 + \frac{A}{T_m^0 - T_c}\right) \tag{17}$$

where σ_{e0} and σ_e are the fold surface enthalpy without and with nucleating agent, respectively, $\Delta H_f/\upsilon_c$ is the melting enthalpy per unit volume, and A (<0) is related to the concentration of nucleating agent. σ_e would be locally decreased with increasing nucleating agent, and the thickness of lamellae should decrease at a given ΔT or T_c. On the other hand, the higher T_c or the lower ΔT leads to a lamellar thickening. The contributions of σ_e and ΔT to the thickness play opposed roles. The present results have shown that ΔT is a dominant factor. Assuming that the volume fraction of the lamellar stacks is almost a constant, the thickening of crystalline lamellae is proportional to the increase in X_c.

The special behavior during the morphological development always emerges at the position of 500 μm. This can be related to a local maximum of pressure in the close vicinity to 500 μm during the packing stage of injection molding.[33] T_c can be shifted by ΔT_c to $T_c + \Delta T_c$ by the pressure jump. As a result, the crystallization rate decreases in the position at T_c but increases in the position at $T_c + \Delta T_c$.[33] Since the temperature increases continuously from the mold wall to the core center, the crystallization at a position should undergo at a relative low temperature between T_c and $T_c + \Delta T_c$. The crystallization rate at such a position cannot reach its maximum. This phenomenon is called as a "pressure quenching", which in this work happens at 500 μm. Consequently, the crystallinity of α-form crystal is dropped to its minimum. As SB is increased to 1.2%, however, the crystallization temperature is increased to such a stage that the "pressure quenching" is not longer significant. On the other hand, it has been known that the conditions for the nucleation and growth of β-form crystal are[34] (a) from an oriented melt, (b) by quick cooling from the melt to 100−125 °C, and (c) high pressure. Apparently, the "pressure quenching" meets these conditions well, which explains the observation of the maximum crystallinity of β-form crystal at the position of 500 μm.

As shown in Figure 1, the orientation functions f_c and f_{a^*} include the contributions of both *c*-axis orientation and *a**-axis orientation from *c*-axis-oriented components and *a**-axis-oriented components. The decrease in f_c with increasing SB in a given position can indicate either that the contribution of *c*-axis orientation from the *c*-axis-oriented components decreases or that the contribution of *c*-axis orientation from the *a**-axis-oriented components increases. The latter is equivalent to the increase in f_{a^*}. Since the *c*-axis of *c*-axis-oriented components is almost perpendicular to the *c*-axis of the *a**-axis-oriented components, as shown in Figure 1, the f_c alone cannot show a relative level of molecular orientation.

The orientation of crystalline lamellae has important implications regarding the molecular orientation. For example, the SAXS fwhm of iPP-1.2 is smaller than that of iPP-0.0 at 200 μm, although the values of f_c are about 0 for iPP-1.2 and 0.3 for iPP-0.0 (see Figure 11). If the chains in a crystalline lamella were randomly oriented to the flow direction, a crystalline lamella would not be constructed and the SAXS fwhm would not be measured from the azimuthal pattern of meridian scattering. It is concluded that the decrease in f_c with SB is only associated with the increase in the amount of *a**-axis-oriented components. The molecular orientation, like lamellar orientation, is in fact enhanced by the addition of SB, which is consistent with our previous report.[35]

The effect of the "pressure quenching" on the molecular orientation is also imprinted at 500, irrespective of SB concentration. Computer simulations and experiments have shown that the flow fields are always essential for the formation of the shish, whereas the kebabs (or the *c*-axis-oriented components) can grow on the shish in the absence of any flow.[36−38] In addition, the studies leading to the morphology shown in Figure 1 suggest that some of polymer chains would be rejected from the kebabs (or *c*-axis-oriented components) before their solidification.[10] Those rejected chains stay in the space between the kebabs and act as nuclei to initiate the second crystallization, leading to the epitaxial growth of *a**-axis-oriented components. The level of shear flow is much attenuated at 500 μm, compared with the positions closer to the skin, and the thermal level is dominant. The faster cooling rate due to the "pressure quenching" causes lower levels of *c*-axis orientation at 500 μm. On the other hand, the chains just squeezed out of the lamellar precursors or "wet" kebabs can possess the segment alignment to some extent. The higher f_{a^*} is attributed to the growth of *a**-axis-oriented components on these squeezed chains.

The SB molecules are distributed in different regions in relation to the orientation and the growth of *a**-axis-oriented components. First, prior to the crystallization, some of SB molecules are aligned along the flow direction, probably in the form of self-assembly. The polymer melt is therefore modified by the ways including a stress concentration, a melt concentration, or deformation.[24,39,40] The polymer segments could drift together on the surfaces of SB to form an overlap region of aligned chains in the direction of the shear flow.[36] Once the overlap regions form, they would spread rapidly over the entire chains to form a complete shish structure.[36] Upon cooling, the SB-modified iPP melt templates the nucleation and growth of kebabs or *c*-axis-oriented components, which induces the higher level of molecular and lamellar orientations. These SB molecules subsequently can remain in the crystalline bulk and the boundary areas between shishes and kebabs.

It is suggested that the second region where the SB molecules could reside be in the basal interfaces of the formed kebabs or *c*-axis-oriented components.[22] According to the literature,[22] the nucleating agent molecules may tend to diffuse toward the formation of basal interfaces, through the some ways of epitaxy, because the extra energy is required for the nucleating agent molecules to diffuse to the amorphous bulk. The existence of nucleating agent molecules in basal interfaces leads to a local decrease in σ_e. If we adopt such a model, the distribution of SB molecules may be schematically shown in Figure 13. These SB molecules could assist the nucleation and growth of *a**-axis-oriented components in the secondary crystallization. Note

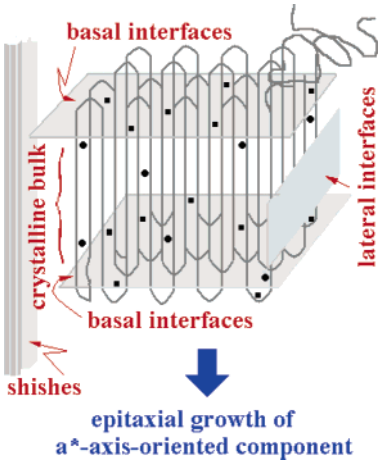

Figure 13. A schematic diagram for the distribution of SB molecules residing in a branched shish-kebab structure.

that for solution-cast iPP/SB films prepared with special procedures the epitaxial crystallization rests on the interaction between SB and the (010) plane of α-phase crystal with a 5 Å periodicity.[41] The epitaxial crystallization of *a**-axis-oriented components in sheared iPP melt should be more complicated. It has been suggested that the lattice matching would not be necessary for the epitaxial crystallization of dense polymer melt under shear.[39,40] The SB molecules residing in the basal interfaces may cause the higher level of orientation of daughter lamellae or *a**-axis-oriented components, analogous to that in the parent lamellae or *c*-axis-oriented components. The SB molecules in the different regions may act independently or in conjunction with each other to varying degrees, depending on the time scale, SB dispersity, and level of shear flow.

The azimuthal patterns of SAXS have shown a slight inclination of the oriented lamellae in the presence of SB. Since the molecular orientation and the lamellar orientation are simultaneously enhanced by the addition of SB, the polymer chains in crystalline lamellae are more oriented to the flow direction, but the lamellar normal of few crystalline lamellae could be slightly inclined with respect to the flow direction. It is suggested from this observation that the inclination of oriented lamellae may be attributed to a chain sliding in boundaries between the shishes and kebabs. The shish walls are composed of stretched segments only without SB but aligned segments and SB molecules in the presence of SB. The mechanisms of SB-mediated inclination of oriented lamellae may be related to the packing density and uneven stress distribution in the lamellar boundaries, although the details are open for debate.

Conclusions

The effects of sodium benzoate on the morphological development of sheared iPP plates prepared under industry scale were investigated using the synchrotron WAXD and SAXS. The experiments were designed in such a way that a microbeam passed through the shear field or temperature gradient, and the illuminated zone was matched to the size of layered structures at a given distance.

The results show that in high concentrations of SB the overall crystallinity slightly decreases in the shear region but increases over a broad range. The increase in the overall crystallinity is attributed to the SB-enhanced crystallization of α-form crystal. An intricate balance between shear flow and local supercooling is believed to control the crystallization. In particular, the minimum crystallinity of α-form crystal does not emerge in the core center but at the position of 500 μm where the maximum crystallinity of β-form crystal is observed. This special behavior of morphological development is attributed to the "pressure quenching" during the packing stage in the course of injection molding. Since the crystallization of α-form crystal at the "pressure quenching" should occur at a relatively low temperature, the crystallization rate of α-form crystal at the position cannot reach its maximum and consequently the crystallinity accordingly decreases. As the concentration of SB is increased to 1.2%, however, the crystallization temperature is increased to such a stage that the effect of "pressure quenching" on the crystallization is not longer significant. On the other hand, the "pressure quenching" provides the favorable conditions for the formation of β-form crystal.

It is found that the decrease in the orientation function f_c with SB indicates the increase in the amount of daughter lamellae or *a**-axis-oriented components. The increase in the amount of daughter lamellae is also evidenced by the increase in the orientation function f_{a^*}. In the absence of SB, the contribution from *c*-axes of parent lamellae or *c*-axis-oriented components would be dominant, which can be reflected in the positive values of f_c. As the SB is added, the daughter lamellae are nucleated by the epitaxial growth and the f_c decreases. When the concentration of SB exceeds a critical value, the contribution from *c*-axes of daughter lamellae is dominant and the f_c becomes a negative. However, the decrease in the orientation function f_c is not necessarily associated with low levels of *c*-axis orientation of parent lamellae or *c*-axis-oriented components. Even though the f_c of α-form crystal is equal to zero and even negative, SAXS data indicate that the *c*-axis orientation of parent lamellae retains in a certain level. The molecular orientation and lamellar orientation of the α-form crystal are increased with increasing SB.

The results show that the thickness of crystalline lamellae increases with increasing depth of plates and concentration of SB. The thickness of crystalline lamellae is determined by the fold surface enthalpy and cooling rate. The cooling rate would play a crucial role in the thickening of crystalline lamellae. Furthermore, the azimuthal patterns of SAXS have shown a slight inclination of the oriented lamellae in the presence of SB. The chain sliding in boundaries between the shishes and kebabs may be attributed to the SB mediation and uneven stress distribution.

Acknowledgment. This work was performed at the Australian National Beamline Facility (ANBF) with support from the Australian Synchrotron Research Program, which is funded by the Commonwealth of Australia under the Major National Research Facilities Program. Dr. James Hester (ANBF) is greatly acknowledged for his assistance in the experiments. P. W. Zhu thanks Dr. Fujiyama for very fruitful discussions.

References and Notes

(1) Meijer, H. E. H., Ed. *Processing of Polymers*; Wiley-VCH: Weinheim, Germany, 1997; Vol. 18.
(2) Janeschitz-Kriegl, H. *Colloid Polym. Sci.* **2003**, *281*, 1157.
(3) Schrauwen, B. A. G.; Breemen, L. C. A.; Spoelstra, A. B.; Govaert, L. E.; Peters, G. W. M.; Meijer, H. E. H. *Macromolecules* **2004**, *37*, 8618.
(4) Mencik, Z.; Fitchmun, D. R. *J. Polym. Sci., Polym. Phys. Ed.* **1973**, *11*, 973.
(5) Viana, J. C. *Polymer* **2004**, *45*, 993.
(6) Kantz, M. R.; Newman, H. D.; Stigale, F. H. *J. Appl. Polym. Sci.* **1972**, *16*, 1249.
(7) Clark, E. S.; Spruiell, J. E. *Polym. Eng. Sci.* **1976**, *16*, 176.
(8) Zipper, P.; Janosi, A.; Wrentschur, E.; Abuja, P. M. *J. Appl. Crystallogr.* **1991**, *24*, 702.
(9) Ulcer, Y.; Cakmak, M. *Polymer* **1997**, *38*, 2907.

(10) Fujiyama, M.; Wakino, T.; Kawasaki, Y. *J. Apply. Polym. Sci.* **1988**, *35*, 129.
(11) Katti, S. S.; Schultz, J. M. *Polym. Eng. Sci.* **1982**, *22*, 1001.
(12) Eder, G.; Janeschitz-Kriegl, H. *Colloid Polym. Sci.* **1988**, *266*, 1087.
(13) Choi, D.; White, J. L. *Polym. Eng. Sci.* **2002**, *42*, 1642.
(14) Sousa, R. A.; Reis, R. L.; Cunha, A. M.; Bevis, M. J. *J. Appl. Polym. Sci.* **2003**, *89*, 2079.
(15) Keller, A.; Kolnaar, H. W. *Mater. Sci. Technol.* **1997**, *18*, 189.
(16) Wunderlich, B. *Macromolecular Physics*; Academic: New York, 1973; Vol. 2.
(17) Somani, R. H.; Yang, L.; Hsiao, B. S.; Agarwal, P. K.; Fruitwala, H. A.; Tsou, A. H. *Macromolecules* **2002**, *35*, 9096.
(18) Lotz, B.; Wittmann, J. C.; Lovinger, A. J. *Polymer* **1996**, *37*, 4979.
(19) Lotz, B.; Wittmann, J. C. *J. Polym. Sci., Part B: Polym. Phys.* **1986**, *24*, 1541.
(20) Kurja, J.; Mehl, N. A. In *Plastics Additives Handbook*, 5th ed.; Zweifei, H., Ed.; Hanser: Munich, Germany, 2001.
(21) Blomenhofer, M.; Ganzleben, S.; Hanft, D.; Schmidt, H.; Kristiansen, M.; Smith, P.; Stoll, K.; Mader, D.; Hoffmann, K. *Macromolecules* **2005**, *38*, 3688.
(22) Alootta, F.; Di Marco, G.; Ober, R.; Pieruccini, M. *J. Appl. Phys.* **2003**, *93*, 2039.
(23) Jang, G.; Cho, W.; Ha, C. *J. Polym. Sci., Part B: Polym. Phys.* **2001**, *39*, 1001.
(24) Reguera, D.; Rubi, J. M. *J. Chem. Phys.* **2003**, *119*, 9888.
(25) Nogales, A.; Mitchell, G. R.; Vaughan, A. S. *Macromolecules* **2003**, *36*, 4898.
(26) Zhu, P. W.; Edward, G. *Macromolecules* **2004**, *37*, 2658.
(27) Turner-Hones, A.; Cobbold, A. J. *Polym. Lett.* **1968**, *6*, 539.
(28) Wilchinsky, Z. W. *J. Appl. Phys.* **1960**, *31*, 1969.
(29) Alexander, L. E. *X-Ray Diffraction Methods in Polymer Science*; Wiley-Interscience: New York, 1976.
(30) Turner-Jones, A.; Aizlewood, J. M.; Beckett, D. R. *Makromol. Chem.* **1964**, *75*, 134.
(31) Tribout, C.; Monasse, B.; Haudin, J. *Colloid Polym. Sci.* **1996**, *274*, 197.
(32) Donth, E. J. *Relaxation and Thermodynamics in Polymers*; Akadenie: Berlin, 1992.
(33) Trotignon, J.; Verdu, J. *J. Appl. Polym. Sci.* **1987**, *34*, 1.
(34) Karger-Kocsis, J., Ed. *Polypropylene: Structure, Blends and Composites*; Chapman & Hall: London, 1995.
(35) Zhu, P. W.; Phillips, A.; Tung, J.; Edward, G. *J. Appl. Phys.* **2005**, *97*, 104908.
(36) Dukovski, I.; Muthukumar, M. *J. Chem. Phys.* **2003**, *118*, 6648.
(37) Hu, W.; Frenkel, D.; Mathot, V. B. F. *Macromolecules* **2002**, *35*, 7172.
(38) Gu, F.; Bu, H.; Zhang, Z. *Macromolecules* **2000**, *33*, 5490.
(39) Misra, A.; Deopura, B. L.; Xavier, S.; Hartley, F. D.; Peters, R. H. *Angew. Makromol. Chem.* **1983**, *113*, 113.
(40) Campbell, D.; White, J. R. *Angew. Makromol. Chem.* **1984**, *122*, 61.
(41) Mathieu, C.; Thierry, A.; Wittmann, J. C.; Lotz, B. *Polymer* **2004**, *41*, 7241.

MA052375G